

# Reanalysis of the binary neutron star merger GW170817 using numerical-relativity calibrated waveform models

Tatsuya Narikawa<sup>1,2,\*</sup>, Nami Uchikata<sup>3,2,†</sup>, Kyohei Kawaguchi<sup>2,4,‡</sup>, Kenta Kiuchi<sup>4,5,§</sup>,  
Koutarou Kyutoku<sup>1,6,7,5,¶</sup>, Masaru Shibata<sup>4,5,\*\*</sup> and Hideyuki Tagoshi<sup>2,††</sup>

<sup>1</sup>*Department of Physics,*

*Kyoto University, Kyoto 606-8502, Japan*

<sup>2</sup>*Institute for Cosmic Ray Research,*

*The University of Tokyo, Chiba 277-8582, Japan*

<sup>3</sup>*Graduate School of Science and Technology,*

*Niigata University, Niigata 950-2181, Japan*

<sup>4</sup>*Max Planck Institute for Gravitational Physics (Albert Einstein Institute),  
Am Mühlenberg 1, Potsdam-Golm 14476, Germany*

<sup>5</sup>*Center for Gravitational Physics,*

*Yukawa Institute for Theoretical Physics,*

*Kyoto University, Kyoto 606-8502, Japan*

<sup>6</sup>*Theory Center, Institute of Particle and Nuclear Studies,*

*KEK, Tsukuba 305-0801, Japan*

<sup>7</sup>*Interdisciplinary Theoretical Science (iTHES) Research Group,*

*RIKEN, Wako, Saitama 351-0198, Japan*

(Dated: November 1, 2019)

We reanalyze gravitational waves from a binary-neutron-star merger GW170817 using a numerical-relativity (NR) calibrated waveform model, the TF2+*KyotoTidal* model. By imposing a uniform prior on the binary tidal deformability  $\tilde{\Lambda}$  the symmetric 90% credible interval of  $\tilde{\Lambda}$  is estimated to be  $481_{-359}^{+436}$  ( $402_{-279}^{+465}$ ) for the case of  $f_{\max} = 1000$  Hz (2048 Hz), where  $f_{\max}$  is the maximum frequency in the analysis. We also reanalyze the event with other waveform models: two post-Newtonian waveform models (TF2+*PNTidal* and TF2+*PNTidal*), the TF2+*MRTidal* model that is another NR calibrated waveform model, and its upgrade, the TF2+*MRTidalv2* model. While estimates of parameters other than  $\tilde{\Lambda}$  are broadly consistent among different waveform models, our results indicate that there is a difference in estimates of  $\tilde{\Lambda}$  among three NR calibrated waveform models. The difference in the peak values of posterior probability density functions of  $\tilde{\Lambda}$  between the NR calibrated waveform models (the TF2+*KyotoTidal* and TF2+*MRTidalv2* models) for  $f_{\max} = 1000$  Hz is about 40 and is much smaller than the width of 90% credible interval, which is about 700. The systematic error for the NR calibrated waveform models will be significant to measure  $\tilde{\Lambda}$  in the case of GW170817-like signal for the planned third generation detectors's sensitivities.

## I. INTRODUCTION

Binary-neutron-star (BNS) mergers are valuable laboratories for nuclear astrophysics. Matter effects influence the orbital evolution and gravitational radiation through the tidal interaction between the neutron stars (NSs) in the late inspiral phase. Additionally, the presence of material gives rise to electromagnetic emission approximately coincident with gravitational radiation. Because these signatures depend on the properties of nuclear matter, their observations allow us to study various nuclear properties such as the equation of state (EOS) for NS matter.

GW170817 [1] and associated electromagnetic counterparts are used to derive various constraints on NS properties and the underlying EOS. The existence of a blue component in the kilonova/macronova AT 2017gfo [2] might suggest that the merger remnant did not collapse promptly to a black hole. Thus, the maximum mass of the NS should not be as small as  $\sim 2M_{\odot}$  [3] and also the radii of high-mass NS may not be very small, e.g., the radius of the maximum-mass configuration is likely to be larger than 9.60 km [4] (but see also Ref. [5]). At the same time, the short gamma-ray burst GRB 170817A [6] and the absence of magnetar-powered emission in AT 2017gfo suggest that the remnant NS collapsed early in the postmerger phase (but see also Refs. [7–10]). Accordingly, a maximum mass of  $\gtrsim 2.3M_{\odot}$  is also unlikely [3, 11–14].

Tidal deformability extracted via cross-correlating gravitational-wave (GW) data of GW170817 with theoretical waveforms gives us more concrete information about the NS than electromagnetic counterparts. The LIGO-Virgo collaborations initially put an upper limit on the binary tidal deformability  $\tilde{\Lambda}$  of the binary as  $\tilde{\Lambda} \lesssim 800$

\* narikawa@tap.scphys.kyoto-u.ac.jp

† uchikata@astro.sc.niigata-u.ac.jp

‡ kkawa@icrr.u-tokyo.ac.jp

§ kenta.kiuchi@aei.mpg.de

¶ kyutoku@tap.scphys.kyoto-u.ac.jp

\*\* mshibata@yukawa.kyoto-u.ac.jp

†† tagoshi@icrr.u-tokyo.ac.jp

with the prior on the dimensionless NS spin being chosen to be  $|\chi| \leq 0.05$  [1]. This limit is later corrected to be  $\tilde{\Lambda} \lesssim 900$  in Ref. [15], where the result of updated analysis is also reported as, e.g.,  $\tilde{\Lambda} = 300_{-230}^{+420}$  for a particular set of assumptions. The constraint can be further improved by assuming the EOS to be common for both NS [16, 17] (but see also Ref. [18]) as is also done in an independent analysis [19, 20]. These constraints are used to investigate the NS EOS [21–23] as well as those for quark and hybrid stars [24–26]. While it has been claimed based on a limited number of numerical-relativity (NR) simulations that  $\tilde{\Lambda} \gtrsim 400$  is necessary to account for the ejecta mass of  $\approx 0.05M_{\odot}$  required to explain AT 2017gfo [27], later systematic investigations reveal that this argument is premature [5].

An accurate theoretical waveform template is crucial to extract accurately the tidal deformability of NSs from the observed GW data. For the early stage of the inspiral, the waveforms including the linear-order tidal effects derived by post-Newtonian (PN) calculation are useful [28, 29]. However, the PN expansion becomes invalid as the orbit becomes relativistic, and thus, the error of the waveform becomes large in the late stage [30–33]. Such errors would cause the systematic bias in the parameter estimation, and it would be in particular problematic for estimating the tidal deformability because the tidal effects on the waveform become most significant just before the merger [34, 35]. The effective-one-body (EOB) formalism can solve this problem by incorporating the higher-order PN correction by re-summation techniques and calibrating them to NR waveforms [34, 36–39]. However, such calibration is performed only focusing on binary black holes (BBHs), and the calibration of the tidal correction employing NR simulation data of BNSs is also required.

Dietrich *et al.* have derived a gravitational waveform model, `NRTidal`, for BNSs based on high-precision NR simulations [40]. Improved reanalyses of GW170817 with more sophisticated waveform models calibrated by NR simulation of BNS merger have been performed employing such a model [15]. Indeed, it is pointed out that the value of the tidal deformability tends to be overestimated if the PN models are employed for the parameter estimation [1]. Recently, its upgrade, the `NRTidalv2` model, which is calibrated by more precise NR waveforms, has been derived [41]. Kawaguchi *et al.* have also developed a model (hereafter the `KyotoTidal` model) for frequency-domain gravitational waveforms of inspiraling BNSs [42]. In particular, this model is derived independently from the `NRTidal` model employing different NR waveforms. Since the `NRTidal` model is so far the only NR calibrated waveform model that is used for parameter estimation of GWs from BNS mergers, the analysis comparing these three NR-calibrated waveform models would help us to understand the systematic biases in resulting constraints on tidal deformability.

In this paper, we reanalyze the data around GW170817 against a NR calibrated waveform model, the `TF2+KyotoTidal` model and present constraints

on the binary tidal deformability. We also reanalyze the event with other waveform models: two PN (`TF2_PNTidal` and `TF2+_PNTidal`), `TF2+_NRTidal`, and `TF2+_NRTidalv2` models.

The remainder of this paper is organized as follows. In Sec. II, we explain the methods for parameter estimation including waveform models used to reanalyze GW170817. In Sec. III, we present results of our analysis of GW170817, a comparison of our analysis with the LIGO-Virgo analysis, and a separate analysis for the LIGO twin detectors. In Sec. IV, we discuss a systematic error in estimation of the binary tidal deformability among waveform models. Section V is devoted to a summary. In Appendix, we present an in-depth study of our results by separate analysis for the LIGO twin detectors to interpret the origin of the complex structure at high- $\tilde{\Lambda}$  region for the posterior probability density function (PDF) of  $\tilde{\Lambda}$  (see also Ref. [43]). Unless otherwise stated, we employ the units  $c = G = 1$ , where  $c$  and  $G$  are the speed of light and the gravitational constant, respectively.

## II. PARAMETER ESTIMATION METHODS

### A. Data and Bayesian inference

We use Bayesian inference to reanalyze GW170817 with various waveform models that incorporate tidal effects in a different manner. Our analysis follows the one performed in our recent work [43], and uses the public data by LVC<sup>1</sup>. We calculate the posterior PDF,  $p(\vec{\theta}|\vec{s}(t), H)$ , for the binary parameters  $\vec{\theta}$  for the gravitational waveform model,  $H$ , given the LIGO Hanford, LIGO Livingston, and Virgo data  $\vec{s}(t)$  via

$$p(\vec{\theta}|\vec{s}(t), H) \propto p(\vec{\theta}|H)p(\vec{s}(t)|\vec{\theta}, H). \quad (1)$$

$p(\vec{\theta}|H)$  is the prior for the binary parameters. The likelihood  $p(\vec{s}(t)|\vec{\theta}, H)$  is evaluated by assuming stationarity and Gaussianity for the detector noise using the noise power spectrum density derived with BayesLine<sup>2</sup>. We compute PDFs by using stochastic sampling engine based on nested sampling [44, 45]. Specifically, we use the parameter estimation software, LALInference [46, 47], which is one of the software of LIGO Algorithm Library (LAL) software suite. We take the frequency range from 23 Hz to  $f_{\max}$ . Here, the maximum frequency  $f_{\max}$  is chosen from two values, 1000 Hz or  $\min[f_{\text{ISCO}}, f_s/2]$ , where  $f_{\text{ISCO}}$  is twice the orbital frequency at the innermost stable circular orbit of a Schwarzschild black hole

<sup>1</sup> <https://www.gw-openscience.org/catalog/GWTC-1-confident/single/GW170817/> for Hanford and Virgo, <https://dcc.ligo.org/LIGO-T1700406/public> for Livingston

<sup>2</sup> <https://dcc.ligo.org/LIGO-P1900011/public>

with total mass of the binary, and  $f_s$  is the sampling rate of data. We set  $f_s = 4096$  Hz. The former choice is made because the **TF2+KyotoTidal** model is calibrated in the frequency range of 10-1000 Hz. The latter choice

corresponds to the assumption that the inspiral stage is terminated at the smaller of  $f_{\text{ISCO}}$  and  $f_s/2$ . In this work, we represent the latter choice by  $f_{\text{max}} = 2048$  Hz for simplicity.

Model name	Point-particle part		Tidal part	
	Amplitude	Phase	Amplitude	Phase
<b>TF2_PNTidal</b>	3PN	3.5PN	5+1PN	5+2.5PN
<b>TF2+_PNTidal</b>	6PN	6PN	5+1PN	5+2.5PN
<b>TF2+_KyotoTidal</b>	6PN	6PN	Polynomial	Nonlinear
<b>TF2+_NRTidal</b>	6PN	6PN	-	Padé approximation
<b>TF2+_NRTidalv2</b>	6PN	6PN	Padé approximation	Padé approximation

TABLE I. Waveform models used to reanalyze GW170817. Our reference model, the **TF2+\_KyotoTidal** model incorporates **TF2+**, as the point-particle and spin parts, and NR calibrated tidal effects. The **TF2** approximant employs the 3.5PN- and 3PN-order formulas for the phase and amplitude, respectively as the point-particle part, and treats aligned spins and incorporates 3.5PN-order formula in spin-orbit interactions, 2PN-order formula in spin-spin, and self-spin interactions. **TF2+** is the **TF2** approximant supplemented with phenomenological higher-order PN terms calibrated by **SEOBNRv2** for the point-particle part. The **TF2+\_NRTidal** model is another model whose tidal effects are calibrated by NR. The **TF2+\_NRTidalv2** model is the upgrade of the **TF2+\_NRTidal** model. The **TF2\_PNTidal** and **TF2+\_PNTidal** models employ the PN tidal-part phase formula.

## B. Waveform models for inspiraling BNSs

We use different analytic frequency-domain waveform models for the inspiral phase. The features of each waveform model are summarized in Table I. The Fourier transform of the gravitational waveform can be written as

$$\tilde{h}(f) = A(f)e^{i\Psi(f)}, \quad (2)$$

where the amplitude  $A(f)$  and the phase  $\Psi(f)$  can be decomposed into the point-particle evolution, the spin effects, and the tidal effects as

$$A(f) = A_{\text{point-particle}}(f) + A_{\text{spin}}(f) + A_{\text{tidal}}(f), \quad (3)$$

and

$$\Psi(f) = \Psi_{\text{point-particle}}(f) + \Psi_{\text{spin}}(f) + \Psi_{\text{tidal}}(f). \quad (4)$$

We use **TaylorF2** [48, 49] (hereafter **TF2**) and phenomenologically extended model of **TF2**, called **TF2+** (see Ref. [42] and below) as BBH baseline, which consists of point-particle and spin parts. Here, the 3.5PN-order formula for the phase and 3PN-order formulas for the amplitude are employed as the point-particle part of **TF2** [50]. For **TF2+**, both the phase and amplitude of the point-particle part are extended to the 6PN-order by fitting the **SEOBNRv2** model [51, 52].

All waveform models used in our parameter estimation analyses assume that the spins of component stars are aligned with the orbital angular momentum, and incorporate 3.5PN-order formula in couplings between the orbital angular momentum and the component spins [53], 2PN-order formula in point-mass spin-spin, and self-spin interactions [54, 55].

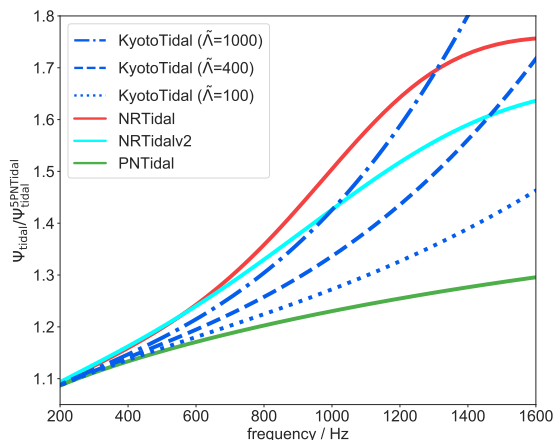


FIG. 1. Tidal phase in the frequency domain normalized by the leading, Newtonian (relative 5PN-order) tidal phase formula. Here, we use  $(m_1, m_2) = (1.35M_\odot, 1.35M_\odot)$ . We show  $\tilde{\Lambda} = 1000$  (dot-dashed, blue), 400 (dashed, blue), and 100 (dotted, blue) for the **KyotoTidal** model. The **NRTidal** model (solid, red), the **NRTidalv2** model (solid, cyan), and the 5+2.5PN-order tidal-part phase formula, **PNTidal** (solid, green), are also presented, which are independent of  $\tilde{\Lambda}$  when normalized by the leading tidal phase.

During the BNS inspiral, at the leading order, the induced quadrupole moment tensor  $Q_{ij}$  is proportional to the external tidal field tensor  $\mathcal{E}_{ij}$  as  $Q_{ij} = -\lambda\mathcal{E}_{ij}$ . The information about the NS EOS can be quantified by the tidal deformability parameter  $\lambda$  [28, 56]. The leading order tidal contribution to the GW phase evolution (rel-

ative 5PN-order) is governed by the symmetric contribution of NS tidal deformation, characterized by the binary tidal deformability [28]

$$\tilde{\Lambda} = \frac{16(m_1 + 12m_2)m_1^4\Lambda_1 + (m_2 + 12m_1)m_2^4\Lambda_2}{13(m_1 + m_2)^5}, \quad (5)$$

which is a mass-weighted linear combination of the tidal deformability of the both components, where  $m_{1,2}$  is the component mass and  $\Lambda_{1,2}$  is the dimensionless tidal deformability parameter of each star  $\Lambda = \lambda/m^5$ . The antisymmetric contribution  $\delta\tilde{\Lambda}$  terms are always subdominant on the tidal effects to the GW phase and the symmetric contribution  $\tilde{\Lambda}$  terms dominate [30, 33]. In this paper, we ignore the  $\delta\tilde{\Lambda}$  contribution.

The `TF2_PNTidal` and `TF2+_PNTidal` models denote the waveform models employing TF2 and TF2+ as the BBH baseline, respectively. Both the `TF2_PNTidal` and the `TF2+_PNTidal` models employ the 2.5PN-order (relative 5+2.5PN-order) tidal-part phase formula [34]

$$\Psi_{\text{tidal}}^{\text{PNTidal}} = \frac{3}{128\eta} \left[ -\frac{39}{2} \tilde{\Lambda} x^{5/2} \times \left( 1 + \frac{3115}{1248} x - \pi x^{3/2} + \frac{28024205}{3302208} x^2 - \frac{4283}{1092} \pi x^{5/2} \right) \right], \quad (6)$$

where  $x = (\pi M_{\text{tot}} f)^{2/3}$  is the dimensionless PN parameter,  $M_{\text{tot}} = m_1 + m_2$  is the total mass, and  $\eta = m_1 m_2 / (m_1 + m_2)^2$  is the symmetric mass ratio. The tidal-part amplitude for both `TF2_PNTidal` and `TF2+_PNTidal` models employ the 5+1PN-order amplitude formula given by [34]

$$A_{\text{tidal}}^{\text{PNTidal}} = \sqrt{\frac{5\pi\eta}{24} \frac{M_{\text{tot}}^2 (1+z)^2}{d_L}} \tilde{\Lambda} x^{-7/4} \times \left( -\frac{27}{16} x^5 - \frac{449}{64} x^6 \right), \quad (7)$$

where  $d_L$  is the luminosity distance to the source and  $z$  is the source redshift.

The `TF2+_KyotoTidal` model is a NR calibrated waveform model for the inspiral phase of BNS mergers [42, 57]. The `TF2+_KyotoTidal` model employs TF2+ as the BBH baseline and extends the 2.5PN-order (relative 5+2.5PN-order) tidal-part phase formula [34] by multiplying  $\tilde{\Lambda}$  by a nonlinear correction to model the tidal part of the GW phase. The functional forms of the tidal-part phase is

$$\Psi_{\text{tidal}}^{\text{KyotoTidal}} = \frac{3}{128\eta} \left[ -\frac{39}{2} \tilde{\Lambda} \left( 1 + a\tilde{\Lambda}^{2/3} x^p \right) \right] x^{5/2} \times \left( 1 + \frac{3115}{1248} x - \pi x^{3/2} + \frac{28024205}{3302208} x^2 - \frac{4283}{1092} \pi x^{5/2} \right), \quad (8)$$

where  $a = 12.55$  and  $p = 4.240$ . The tidal-part amplitude is extended by adding the higher-order PN tidal effects

to Eq. (7) as

$$A_{\text{tidal}}^{\text{KyotoTidal}} = \sqrt{\frac{5\pi\eta}{24} \frac{M_{\text{tot}}^2 (1+z)^2}{d_L}} \tilde{\Lambda} x^{-7/4} \times \left( -\frac{27}{16} x^5 - \frac{449}{64} x^6 - b x^r \right), \quad (9)$$

where  $b = 4251$  and  $r = 7.890$ . In the `KyotoTidal` model, the hybrid waveforms constructed from high-precision NR waveforms and the `SEOBNRv2T` waveforms [51, 52, 58–60] are used for model calibration in the frequency range of 10-1000 Hz. The phase difference between the `TF2+_KyotoTidal` model and the hybrid waveforms is smaller than 0.1 rad up to 1000 Hz for  $300 \lesssim \tilde{\Lambda} \lesssim 1900$  and for the mass ratio  $q = m_2/m_1 \leq 1$  between 0.73 and 1 [42]. In [42], it is shown that the mismatch between the `TF2+_KyotoTidal` model and the hybrid waveforms is always smaller than  $1.1 \times 10^{-5}$  in the frequency range of 10-1000 Hz.

The `NRTidal` model is another approach to describe tidal effects calibrated by NR waveforms [40]. The `TF2+_NRTidal` model employs TF2+ as the BBH baseline. For the tidal effects, this model extends the linear-order effects by effectively adding the higher-order PN terms of the tidal contribution to the GW phase. As shown in Ref. [40], the expression of the tidal phase is given by the form of a rational function:

$$\Psi_{\text{tidal}}^{\text{NRTidal}} = \frac{3}{128\eta} \left[ -\frac{39}{2} \tilde{\Lambda} x^{5/2} \times \frac{1 + \tilde{n}_1 x + \tilde{n}_{3/2} x^{3/2} + \tilde{n}_2 x^2 + \tilde{n}_{5/2} x^{5/2}}{1 + \tilde{d}_1 x + \tilde{d}_{3/2} x^{3/2}} \right], \quad (10)$$

where  $\tilde{d}_1 = \tilde{n}_1 - 3115/1248$ , the other parameters are  $(\tilde{n}_1, \tilde{n}_{3/2}, \tilde{n}_2, \tilde{n}_{5/2}) = (-17.428, 31.867, -26.414, 62.362)$  and  $\tilde{d}_{3/2} = 36.089$ . We do not consider the tidal-part amplitude for this model following the original form [40].

The `TF2+_NRTidalv2` model is an upgrade of the `TF2+_NRTidal` model [41]. Specifically, they derive a new expression for the tidal phase which is calibrated to more accurate NR waveforms,

$$\Psi_{\text{tidal}}^{\text{NRTidalv2}} = \frac{3}{128\eta} \left[ -\frac{39}{2} \tilde{\Lambda} x^{5/2} \times \frac{1 + \tilde{n}'_1 x + \tilde{n}'_{3/2} x^{3/2} + \tilde{n}'_2 x^2 + \tilde{n}'_{5/2} x^{5/2} + \tilde{n}'_3 x^3}{1 + \tilde{d}'_1 x + \tilde{d}'_{3/2} x^{3/2} + \tilde{d}'_2 x^2} \right], \quad (11)$$

with  $\tilde{n}'_1 = \tilde{c}'_1 + \tilde{d}'_1$ ,  $\tilde{n}'_{3/2} = (\tilde{c}'_1 \tilde{c}'_{3/2} - \tilde{c}'_{5/2} - \tilde{c}'_{3/2} \tilde{d}'_1 + \tilde{n}'_{5/2}) / \tilde{c}'_1$ ,  $\tilde{n}'_2 = \tilde{c}'_2 + \tilde{c}'_1 \tilde{d}'_1 + \tilde{d}'_2$ ,  $\tilde{d}'_{3/2} = -(\tilde{c}'_{5/2} + \tilde{c}'_{3/2} \tilde{d}'_1 - \tilde{n}'_{5/2}) / \tilde{c}'_1$ , where the known coefficients are  $\tilde{c}'_1 = 3115/1248$ ,  $\tilde{c}'_{3/2} = -\pi$ ,  $\tilde{c}'_2 = 28024205/3302208$ ,  $\tilde{c}'_{5/2} = -4283\pi/1092$ , and the fitting coefficients are  $\tilde{n}'_{5/2} = 90.550822$ ,  $\tilde{n}'_3 =$

$-60.253578$ ,  $\tilde{d}'_1 = -15.111208$ ,  $\tilde{d}'_2 = 8.0641096$ . They also introduce the tidal amplitude,

$$A_{\text{tidal}}^{\text{NRTidalv2}} = \sqrt{\frac{5\pi\eta}{24}} \frac{M_{\text{tot}}^2 (1+z)^2}{d_L} \tilde{\Lambda} x^{-7/4} \times \left( -\frac{27}{16} x^5 \right) \frac{1 + \frac{449}{108} x + \frac{22672}{9} x^{2.89}}{1 + dx^4}, \quad (12)$$

where  $d = 13477.8$ .

In Fig. 1, we show differences in the phase evolution of tidal part among the `KyotoTidal`, `NRTidal`, `NRTidalv2`, and `PNTidal` models. A difference in the treatment of the tidal effects makes different  $\tilde{\Lambda}$ -dependence. The tidal phase normalized by the leading (relative 5PN-order) tidal phase formula for the `KyotoTidal` model depends on the binary tidal deformability  $\tilde{\Lambda}$  due to the nonlinear correction. Since the `NRTidal`, `NRTidalv2`, and `PNTidal` models employ the linear-order effects of the tidal deformability, they are independent of  $\tilde{\Lambda}$  when normalized by the leading tidal effect. Figure 1 shows good agreement between the `TF2+KyotoTidal` model and the `TF2+NRTidalv2` model for  $\tilde{\Lambda} \simeq 1000$  below 1000 Hz as suggested in Ref. [41]. The `NRTidal` model gives the largest phase shift, the second is the `NRTidalv2` model, the third is the `KyotoTidal` model, and the `PNTidal` model gives the smallest, for  $\tilde{\Lambda} \leq 1000$ , up to  $\sim 1000$  Hz. The `TF2+KyotoTidal` model is calibrated only up to 1000 Hz and overestimates tidal effects at frequencies above 1000 Hz. The `KyotoTidal` model gives the largest phase shift at frequency above 1200 Hz for  $\tilde{\Lambda} = 1000$ , and larger phase shift than the one for the `NRTidalv2` model at frequency above about 1000 Hz (1400 Hz) for  $\tilde{\Lambda} = 1000$  (400).

### C. Source parameters

The source parameters and their prior probability distributions are chosen to follow those adopted in our recent work [43], and we mention specific choices made in this work.

We fix the sky location to the position of AT 2017gfo, which is an electromagnetic counterpart of GW170817 [61], for all of our analyses and estimates of the remaining source parameters. Specifically, we estimate the luminosity distance to the source  $d_L$ , the binary inclination  $\theta_{\text{JN}}$ , which is the angle between the total angular momentum and the line of sight, the polarization angle  $\psi$ , the coalescence time  $t_c$ , the phase at the coalescence time  $\phi_c$ , component masses  $m_{1,2}$ , where we assume  $m_1 \geq m_2$ , the orbit-aligned dimensionless spin components of the stars  $\chi_{1,2}$  where  $\chi_{1,2} = cS_{1,2}/(Gm_{1,2}^2)$  is the orbit-aligned dimensionless spin components of the stars with  $S_{1,2}$  are the magnitudes of the spin angular momenta of the components, and the binary tidal deformability  $\tilde{\Lambda}$ .

For our analysis, we assume a uniform distribution as the detector-frame component mass prior  $m_{1,2} \sim$

$U[0.83, 7.7]M_{\odot}$  with an additional constraint on the detector-frame chirp mass  $\mathcal{M}^{\text{det}} \sim U[1.184, 2.168]M_{\odot}$ , where the chirp mass is the best estimated mass parameter defined as  $\mathcal{M} = (m_1 m_2)^{3/5} (m_1 + m_2)^{-1/5}$ . The prior range for  $\mathcal{M}^{\text{det}}$  is the same as that used for LIGO-Virgo analysis [15]. The impact of wider prior range for  $\mathcal{M}^{\text{det}}$  on parameter estimation is negligible. We assume a uniform prior on the spin magnitudes and we enforce  $\chi_{1,2} \sim U[-0.05, 0.05]$ . This prior range of spin is consistent with the observed population of known BNSs that will merge within the Hubble time [62, 63], and is referred to as low-spin prior for the LIGO-Virgo analysis [15]. We assume a uniform prior on the binary tidal deformability, with  $\tilde{\Lambda} \sim U[0, 3000]$ .

## III. RESULTS

### A. Source properties other than the tidal deformability

In this subsection, we show validity of our analysis as a sanity check by comparison with the LIGO-Virgo results. Figure 2 shows the marginalized posterior PDFs of parameters other than the tidal deformability for different waveform models for  $f_{\text{max}} = 1000$  Hz. Table II presents the 90% credible intervals of the luminosity distance  $d_L$ , the binary inclination  $\theta_{\text{JN}}$ , mass parameters (the component masses  $m_{1,2}$ , the detector-frame chirp mass  $\mathcal{M}^{\text{det}}$ , the source-frame chirp mass  $\mathcal{M}$ , the total mass  $M_{\text{tot}}$ , and the mass ratio  $q$ ), and the effective spin parameter  $\chi_{\text{eff}} = (m_1 \chi_1 + m_2 \chi_2)/M_{\text{tot}}$ , which is the most measurable combination of spin components, estimated using different waveform models. The source-frame chirp mass is derived by assuming a value of the Hubble constant  $H_0 = 69 \text{ km s}^{-1} \text{ Mpc}^{-1}$  (a default value in LAL).

For comparison of our analysis with the results of the previous LIGO-Virgo analysis [15, 64], we also analyze GW170817 by using the restricted TF2 approximant as the waveform model with 5+1PN-order tidal-part phase formula. This model has the BBH baseline whose amplitude is constructed only from the Newtonian-order point-particle evolution [48, 49, 53–55] and is implemented in LALInference. We checked that estimates of parameters other than the tidal deformability we obtained by using the restricted TF2 model are broadly consistent with the LIGO-Virgo results presented in [15, 64].

The estimates of parameters other than the tidal deformability presented in Fig. 2 and Table II show almost no systematic bias associated with a difference among waveform models for both BBH baseline and tidal parts. The posterior PDFs of these parameters for  $f_{\text{max}} = 2048$  Hz are almost the same as the ones for  $f_{\text{max}} = 1000$  Hz as illustrated for the `TF2_PNTidal` model in Fig. 2. This is due to the fact that the parameters other than the tidal deformability are mainly measured from information at low frequency region [34] and terms up to 3.5PN-order of the point-particle part for the phase

are the same among different waveforms. On the other hand, the tidal deformability is mainly measured from

information at high frequency region as discussed in the next section and below.

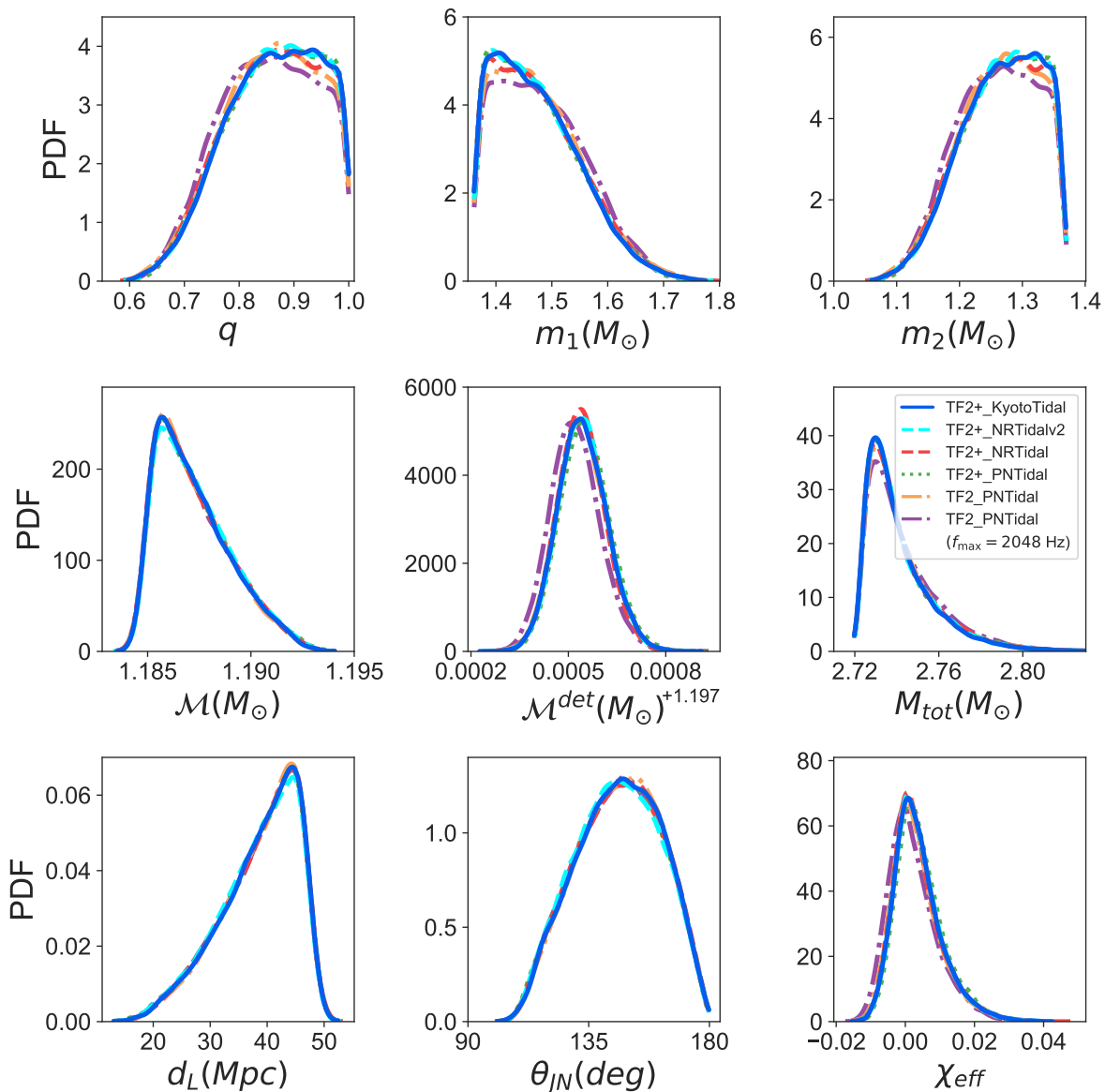


FIG. 2. Marginalized posterior PDFs of various parameters derived by different waveform models. The blue, cyan, red, green, and orange curves correspond to the `TF2+_KyotoTidal`, `TF2+_NRTidalv2`, `TF2+_NRTidal`, `TF2+_PNTidal`, and `TF2_PNTidal` models, respectively. The top-left, top-middle, top-right, middle-left, center, middle-right, bottom-left, bottom-middle, and bottom-right panels show the mass ratio  $q$ , the primary mass  $m_1$ , the secondary mass  $m_2$ , the source-frame chirp mass  $\mathcal{M}$ , the detector-frame chirp mass  $\mathcal{M}_{\text{det}}$ , the total mass  $M_{\text{tot}}$ , the luminosity distance to the source  $d_L$ , the inclination angle  $\theta_{JN}$ , and the effective spin parameter  $\chi_{\text{eff}}$ , respectively. Here, we show the distribution for  $f_{\text{max}} = 1000$  Hz, except for the `TF2_PNTidal` model, for which the intervals for both  $f_{\text{max}} = 1000$  Hz and  $f_{\text{max}} = 2048$  Hz are given.

	TF2_PNTidal	TF2+_PNTidal	TF2+_KyotoTidal	TF2+_NRTidal	TF2+_NRTidalv2
Luminosity distance $d_L$ [Mpc]	$40.0^{+7.3}_{-14.4}$	$39.8^{+7.5}_{-14.7}$	$39.9^{+7.3}_{-14.6}$	$39.9^{+7.4}_{-14.5}$	$39.6^{+7.7}_{-14.6}$
Binary inclination $\theta_{\text{JN}}$ [degree]	$147^{+24}_{-32}$	$146^{+24}_{-27}$	$147^{+24}_{-28}$	$147^{+24}_{-27}$	$146^{+25}_{-27}$
Detector-frame chirp mass $\mathcal{M}^{\text{det}}$ [ $M_{\odot}$ ]	$1.1975^{+0.0001}_{-0.0001}$	$1.1975^{+0.0001}_{-0.0001}$	$1.1975^{+0.0001}_{-0.0001}$	$1.1975^{+0.0001}_{-0.0001}$	$1.1975^{+0.0001}_{-0.0001}$
Source-frame chirp mass $\mathcal{M}$ [ $M_{\odot}$ ]	$1.187^{+0.004}_{-0.002}$	$1.187^{+0.004}_{-0.002}$	$1.187^{+0.004}_{-0.002}$	$1.187^{+0.004}_{-0.002}$	$1.187^{+0.004}_{-0.002}$
Primary mass $m_1$ [ $M_{\odot}$ ]	(1.36, 1.59)	(1.36, 1.58)	(1.36, 1.58)	(1.36, 1.59)	(1.36, 1.58)
Secondary mass $m_2$ [ $M_{\odot}$ ]	(1.18, 1.37)	(1.18, 1.37)	(1.18, 1.37)	(1.18, 1.37)	(1.18, 1.37)
Total mass $M_{\text{tot}} := m_1 + m_2$ [ $M_{\odot}$ ]	$2.74^{+0.04}_{-0.01}$	$2.74^{+0.04}_{-0.01}$	$2.74^{+0.04}_{-0.01}$	$2.74^{+0.04}_{-0.01}$	$2.74^{+0.04}_{-0.01}$
Mass ratio $q := m_2/m_1$	(0.74, 1.00)	(0.74, 1.00)	(0.75, 1.00)	(0.75, 1.00)	(0.75, 1)
Effective spin $\chi_{\text{eff}}$	$0.002^{+0.015}_{-0.009}$	$0.003^{+0.015}_{-0.009}$	$0.003^{+0.014}_{-0.008}$	$0.002^{+0.015}_{-0.008}$	$0.003^{+0.014}_{-0.008}$

TABLE II. 90% credible interval of the luminosity distance  $d_L$ , the binary inclination  $\theta_{\text{JN}}$ , mass parameters, and the effective spin parameter  $\chi_{\text{eff}}$  estimated using different waveform models. We show 10%-100% regions of the mass ratio with the upper limit  $q = 1$  imposed by definition, and those of  $m_1$  and  $m_2$  are given accordingly. We give symmetric 90% credible intervals, i.e., 5%-95%, for the other parameters with the median as a representative value.

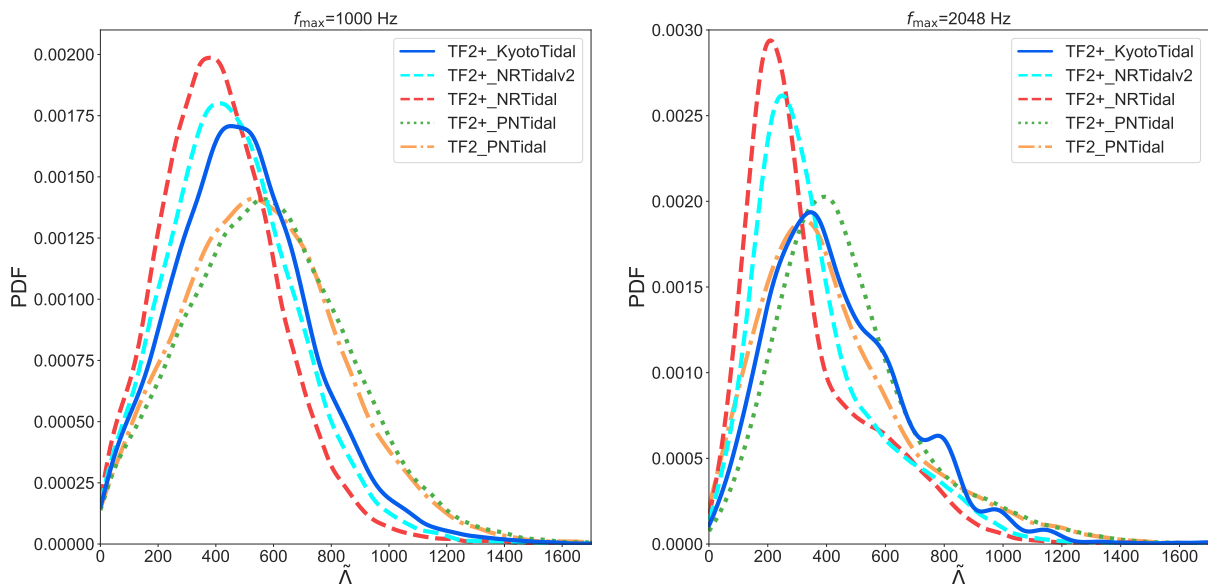


FIG. 3. Marginalized posterior PDFs of binary tidal deformability,  $\tilde{\Lambda}$ , estimated by different waveform models, for both  $f_{\text{max}} = 1000$  Hz (left panel) and 2048 Hz (right panel). The blue, cyan, red, green, and orange curves correspond to the TF2+\_KyotoTidal, TF2+\_NRTidalv2, TF2+\_NRTidal, TF2+\_PNTidal, and TF2\_PNTidal models, respectively. The corresponding 90% credible intervals are presented in Table III.

## B. Posterior of binary tidal deformability

Before presenting our results obtained with various waveform models, we first compare our results obtained by using the restricted TF2 model that incorporates the

5+1PN-order tidal-part phase with those from the LIGO-Virgo analysis [15] as a sanity check. While our result of 90% credible symmetric (highest posterior density (HPD)) interval on  $\tilde{\Lambda}$  is  $347^{+564}_{-243}$  ( $347^{+453}_{-295}$ ) for restricted TF2 with 5+1PN-order tidal-part phase, low-spin prior

Model	$f_{\max} = 1000$ Hz		$f_{\max} = 2048$ Hz	
	Symmetric	HPD	Symmetric	HPD
TF2_PNTidal	548 <sup>+500</sup> <sub>-415</sub>	548 <sup>+433</sup> <sub>-463</sub>	376 <sup>+584</sup> <sub>-284</sub>	376 <sup>+442</sup> <sub>-353</sub>
TF2+_PNTidal	569 <sup>+496</sup> <sub>-431</sub>	569 <sup>+441</sup> <sub>-470</sub>	428 <sup>+540</sup> <sub>-280</sub>	428 <sup>+414</sup> <sub>-353</sub>
TF2+_KyotoTidal	481 <sup>+436</sup> <sub>-359</sub>	481 <sup>+379</sup> <sub>-402</sub>	402 <sup>+465</sup> <sub>-279</sub>	402 <sup>+419</sup> <sub>-316</sub>
TF2+_NRTidal	403 <sup>+378</sup> <sub>-299</sub>	403 <sup>+328</sup> <sub>-337</sub>	267 <sup>+491</sup> <sub>-180</sub>	267 <sup>+409</sup> <sub>-228</sub>
TF2+_NRTidalv2	445 <sup>+412</sup> <sub>-330</sub>	445 <sup>+357</sup> <sub>-370</sub>	312 <sup>+498</sup> <sub>-208</sub>	312 <sup>+407</sup> <sub>-263</sub>

TABLE III. 90% credible interval of the binary tidal deformability,  $\tilde{\Lambda}$ , for different waveform models. We report both the symmetric 90% credible interval (Symmetric) and the 90% highest-posterior-density intervals (HPD), for both  $f_{\max} = 1000$  Hz (left side) and 2048 Hz (right side), where the median is shown as a representative value.

( $|\chi_{1,2}| \leq 0.05$ ), and  $f_{\max} = 2048$  Hz, the LIGO-Virgo collaborations report  $\tilde{\Lambda} = 340^{+580}_{-240}$  ( $340^{+490}_{-290}$ ) in [15]. Here, uniform priors in  $\Lambda_1$  and  $\Lambda_2$  are adopted in both analyses, and the posterior of  $\tilde{\Lambda}$  is divided by its prior determined by those of other parameters following [15] to derive the results for the case of a uniform prior on  $\tilde{\Lambda}$ . The closeness of the inferred credible ranges indicates that our analysis successfully reproduces the results derived by the LIGO-Virgo collaborations. If we assume a uniform prior on  $\tilde{\Lambda}$ , 90% credible symmetric (HPD) interval on  $\tilde{\Lambda}$  is  $316^{+504}_{-224}$  ( $316^{+367}_{-291}$ ) for restricted TF2 with 5+1PN-order tidal-part phase.

Figure 3 shows the marginalized posterior PDFs for the binary tidal deformability  $\tilde{\Lambda}$  for different waveform models for both  $f_{\max} = 1000$  Hz (left panel) and 2048 Hz (right panel). The corresponding 90% credible intervals are presented in Table III. We caution that the TF2+\_KyotoTidal model is calibrated only up to 1000 Hz and can overestimate tidal effects at frequencies above 1000 Hz. Thus, the results for  $f_{\max} = 2048$  Hz should be regarded as only a reference.

For  $f_{\max} = 1000$  Hz (left panel of Fig. 3), the peak values of  $\tilde{\Lambda}$  are 400-500 and the 90% credible intervals do not extend to  $\gtrsim 900$  for NR calibrated waveform models: the TF2+\_KyotoTidal, TF2+\_NRTidalv2, and TF2+\_NRTidal models. Our results show that the posterior of binary tidal deformability for GW170817 are biased by using different waveform models. The TF2+\_KyotoTidal, TF2+\_NRTidal, TF2+\_NRTidalv2, and TF2+\_PNTidal models are constructed from the same BBH baseline, TF2+, but with different tidal descriptions. Therefore, a difference of estimates among these waveform models reflects directly their different tidal description. The TF2+\_NRTidal model gives the smallest median value on  $\tilde{\Lambda}$  of 403, the second is the TF2+\_NRTidalv2 model of 445, the third is the TF2+\_KyotoTidal model of 481, and the TF2+\_PNTidal model gives the largest one of 569. This order is derived from the order of the phase shift of different waveform models for a given value of  $\tilde{\Lambda} = 400$ , up to about 1400 Hz as shown in Fig. 1. The tendency to give smaller estimated values for NR calibrated waveform models than for PN waveform models are consistent with previous results derived in Ref. [65] (see also Ref. [66] for

the detail study of systematic biases associated with spin effects). The TF2+\_PNTidal and TF2\_PNTidal models are constructed from the same tidal part and the different point-particle part. A difference in the posterior PDFs of estimated  $\tilde{\Lambda}$  between these models are very small for  $f_{\max} = 1000$  Hz. This result shows that the higher-order point-particle terms do not significantly affect the estimate of the binary tidal deformability of GW170817 for  $f_{\max} = 1000$  Hz.

For  $f_{\max} = 2048$  Hz (right panel of Fig. 3), the peak values of  $\tilde{\Lambda}$  are 250-400 and the 90% credible intervals do not extend to  $\gtrsim 850$  for NR calibrated waveform models. The width of symmetric 90% credible intervals for  $f_{\max} = 2048$  Hz are narrower than those for  $f_{\max} = 1000$  Hz, by about 7% for the TF2+\_KyotoTidal model, 4% for the TF2+\_NRTidal model, 5% for the TF2+\_NRTidalv2 model, 13% for the TF2+\_PNTidal model, and about 5% for the TF2\_PNTidal model, as shown in Table III. These decrease in the width of the interval are consistent with the fact that higher-frequency data are more informative to measure  $\tilde{\Lambda}$  [34]. The peak values of the posterior PDFs of  $\tilde{\Lambda}$  tend to decrease as  $f_{\max}$  increases for all waveform models as shown in Fig. 3. The order of peak values of  $\tilde{\Lambda}$  for the different waveform models that incorporate the same BBH baseline, TF2+, is not affected by varying  $f_{\max}$  as shown in Fig. 3. This is explained by the same reason as that for  $f_{\max} = 1000$  Hz. We note that 1400 Hz approximately corresponds to  $f_{\text{ISCO}}$  for estimated mass range. The TF2\_PNTidal model gives slightly smaller peak value than the TF2+\_KyotoTidal model. This cannot be explained only by the feature of the tidal part as shown in Fig. 1. This might be due to the effects of the higher-order point-particle terms or the fact that the data at frequencies above 1000 Hz are dominated by the detector's noise. The difference in the posterior PDFs of estimated  $\tilde{\Lambda}$  between the TF2+\_PNTidal and TF2\_PNTidal models for  $f_{\max} = 2048$  Hz is larger than that for  $f_{\max} = 1000$  Hz (see Fig. 3 and Table III). This is due to the effects of higher-order point-particle terms as discussed in [31].

## IV. DISCUSSION

In this section, we discuss the systematic error for waveform models with respect to estimation of the binary tidal deformability. There is a difference among peaks of different waveform models, while the statistical error for the measurement of the binary tidal deformability  $\tilde{\Lambda}$  is much larger than the difference among the peaks for GW170817 (see Fig. 3 and Table III). Here, we use differences in the peak values of the posterior PDFs of  $\tilde{\Lambda}$  as an indicator of the systematic error.

For  $f_{\max} = 1000$  Hz, there are differences in the peak values of  $\tilde{\Lambda}$ , by about 40 between NR calibrated waveform models (the `TF2+KyotoTidal` and `TF2+NRTidalv2` models) and by about 110 between NR calibrated waveform and PN waveform models (the `TF2+KyotoTidal` and `TF2+PNTidal` models). The statistical errors (the width of 90% HPD interval) of the binary tidal deformability  $\tilde{\Lambda}$  are about 700 for NR calibrated models and about 900 for PN waveform models. We note that the systematic error of  $\tilde{\Lambda}$  among different waveform models do not depend on the signal-to-noise ratio (SNR), while the statistical error is proportional to the inverse of SNR for realistic cases. Assuming the detector sensitivity curves at the detection of GW170817, our results suggest that for a signal that has SNR louder than GW170817 (SNR = 32.6) by a factor of about 8, the difference in extraction of  $\tilde{\Lambda}$  between the `TF2+KyotoTidal` model and the `TF2+PNTidal` model can be significant. Comparing the `TF2+KyotoTidal` with `TF2+NRTidalv2` models, the systematic error of  $\tilde{\Lambda}$  can be comparable to the statistical error for a higher SNR signal than GW170817 by a factor of about 18. The planned third generation of GW interferometers, e.g., the Einstein Telescope [67–69] or the Cosmic Explorer [70], will provide an opportunity to observe BNS mergers with more than ten times higher SNR than GW170817. Since for GW170817-like signal for the third generation of GW interferometers the systematic error of  $\tilde{\Lambda}$  can be comparable to the statistical error between the `TF2+KyotoTidal` and `TF2+NRTidalv2` models, it is needed to improve current waveform models. We leave the study of injecting hybrid waveform signals into the noise assuming the planned third generation detectors’s sensitivities and verifying how well current waveform models recover the injected values for future work.

$\tilde{\Lambda}$  is indeed determined more precisely for all waveform models in our analysis for  $f_{\max} = 2048$  Hz than for  $f_{\max} = 1000$  Hz as indicated in Sec. III. However, since the `TF2+KyotoTidal` model is calibrated by hybrid waveforms only up to 1000 Hz, it is needed to further improve the model in the frequency higher than 1000 Hz, toward the third generation detector era.

## V. SUMMARY

We reanalyze GW170817 with a NR calibrated waveform model, the `TF2+KyotoTidal` model. The `TF2+KyotoTidal` model is calibrated in the frequency range of 10-1000 Hz by hybrid waveforms composed of high-precision NR waveforms and the `SEOBNRv2T` waveforms, and reproduces the phase of the hybrid waveforms within 0.1 rad error up to 1000 Hz. In the `TF2+KyotoTidal` model, the nonlinear effects of the tidal deformability is incorporated. We also reanalyze the event with other waveform models: two PN waveform models (`TF2+PNTidal` and `TF2+NRTidal`), the `TF2+NRTidal` model that is another NR calibrated waveform model, and its upgrade, the `TF2+NRTidalv2` model.

We compare parameter estimation results with different tidal waveform models. For GW170817, there seems to be almost no systematic biases for extraction of source parameters other than the binary tidal deformability using different waveform models. We find that the PN model tends to overestimate  $\tilde{\Lambda}$  compared to the NR calibrated waveform models, while there are also the differences in the estimates of  $\tilde{\Lambda}$  among NR calibrated waveform models for  $f_{\max} = 1000$  Hz. For a higher SNR signal than GW170817 by a factor of about 18, the difference in the measurement of the binary tidal deformability  $\tilde{\Lambda}$  between the `TF2+KyotoTidal` and `TF2+NRTidalv2` models can be significant. Therefore, toward the third generation detector era, it is needed to improve current waveform models.

Our results indeed indicate that  $\tilde{\Lambda}$  is constrained more tightly for  $f_{\max} = 2048$  Hz than for  $f_{\max} = 1000$  Hz. For the `TF2+KyotoTidal` model, the 90% symmetric interval of  $\tilde{\Lambda}$  for  $f_{\max} = 2048$  Hz is about 7% narrower than that for  $f_{\max} = 1000$  Hz. Though the estimate of  $\tilde{\Lambda}$  becomes narrower as the  $f_{\max}$  increases, the `TF2+KyotoTidal` model is calibrated only up to 1000 Hz. Since higher frequency data are more informative for  $\tilde{\Lambda}$  [34], it is important to improve current waveform models at high-frequencies above 1000 Hz to accurately determine  $\tilde{\Lambda}$  from the GW data, toward third generation detector era.

## ACKNOWLEDGMENT

We thank John Veitch for very helpful explanation of LALInference and Chris van den Broeck for useful discussions. This work is supported by Japanese Society for the Promotion of Science (JSPS) KAKENHI Grant Numbers JP15K05081, JP16H02183, JP16H06341, JP16H06342, JP17H01131, JP17H06133, JP17H06358, JP17H06361, JP17H06364, JP18H01213, JP18H04595, JP18H05236, and JP19K14720, and by a post-K project hp180179. This work is also supported by JSPS Core-to-Core Program A. Advanced Research Networks and by the joint research program of the Institute for Cosmic Ray Research, University of Tokyo, Computing Infrastructure

Project of KISTI-GSDC in Korea, and Computing Infrastructure ORION in Osaka City University. T. Narikawa is supported in part by a Grant-in-Aid for JSPS Research Fellows, and he also thanks hospitality of Chris's group during his stay at Nikhef. K. Kawaguchi was supported in part by JSPS overseas research fellowships. We are also grateful to the LIGO-Virgo collaborations for the public release of GW data of GW170817. This research has made use of data, software, and web tools ob-

tained from the Gravitational Wave Open Science Center (<https://www.gw-openscience.org>), a service of LIGO Laboratory, the LIGO Scientific Collaboration and the Virgo Collaboration. LIGO is funded by the U. S. National Science Foundation. Virgo is funded by the French Centre National de la Recherche Scientifique (CNRS), the Italian Istituto Nazionale di Fisica Nucleare (INFN), and the Dutch Nikhef, with contributions by Polish and Hungarian institutes.

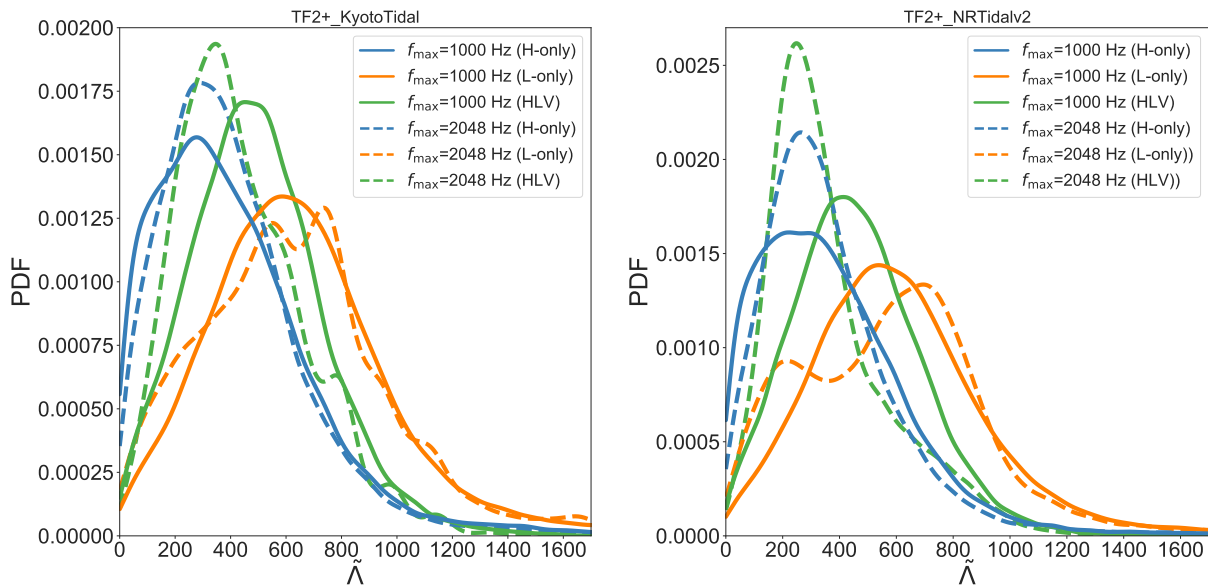


FIG. 4. Marginalized posterior PDFs of binary tidal deformability,  $\tilde{\Lambda}$ , derived by data of different detector combinations with both  $f_{\max} = 1000$  Hz (solid) and 2048 Hz (dashed) for the TF2+\_KyotoTidal (left panel) and the TF2+\_NRTidalv2 (right panel) models. The distribution derived by the Hanford-only data (blue), that by the Livingston-only data (orange), and that by combined data of Advanced LIGO twin detectors and Advanced Virgo (green, denoted by HLV) are presented. For  $f_{\max} = 2048$  Hz, a multimodal (bump) structure at high- $\tilde{\Lambda}$  for the TF2+\_KyotoTidal (TF2+\_NRTidalv2) model appear due to Livingston data.

### Appendix A: Separate analysis for the LIGO twin detectors

There is a multimodal structure at the high- $\tilde{\Lambda}$  region in the posterior PDF of  $\tilde{\Lambda}$  for the TF2+\_KyotoTidal model and a bump structure for the TF2+\_NRTidal and TF2+\_NRTidalv2 models for  $f_{\max} = 2048$  Hz as shown in the right panel of Fig. 3. In this appendix, we present an in-depth study to interpret these features by separate analysis for the LIGO twin detectors. Figure 4 shows marginalized posterior of  $\tilde{\Lambda}$  derived by separate analysis for the Hanford and Livingston de-

tectors with both  $f_{\max} = 1000$  Hz and 2048 Hz for the TF2+\_KyotoTidal model (left panel) and the TF2+\_NRTidalv2 model (right panel). Table IV shows corresponding 90% credible interval of  $\tilde{\Lambda}$ .

In the case of the TF2+\_KyotoTidal model, the left panel in Fig. 4 suggests that the origin of the bump at high- $\tilde{\Lambda}$  region for  $f_{\max} = 2048$  Hz for the HLV combined data is as follows. On the one hand, for the Livingston data, the unimodal distribution for  $f_{\max} = 1000$  Hz, whose peak is at about 600, is separated into a bimodal distribution for  $f_{\max} = 2048$  Hz that is constructed from twin peaks, a low- $\tilde{\Lambda}$  bump, and a few high- $\tilde{\Lambda}$  bumps.

TABLE IV. 90% credible interval of binary tidal deformability,  $\tilde{\Lambda}$ , with the TF2+*KyotoTidal* (left side) and the TF2+*NRTidalv2* (right side) models, for different detector data and the maximum frequency,  $f_{\max}$ . The upper group shows the symmetric intervals and the lower shows the HPD intervals, where the median is shown as a representative value for both groups.

$f_{\max}$	TF2+ <i>KyotoTidal</i>		TF2+ <i>NRTidalv2</i>	
	Hanford-only	Livingston-only	Hanford-only	Livingston-only
	Symmetric			
1000 Hz	$357^{+568}_{-311}$	$618^{+637}_{-447}$	$333^{+514}_{-291}$	$582^{+586}_{-413}$
2048 Hz	$362^{+514}_{-295}$	$607^{+658}_{-482}$	$320^{+481}_{-253}$	$589^{+549}_{-487}$
	HPD			
1000 Hz	$357^{+414}_{-357}$	$618^{+502}_{-523}$	$333^{+378}_{-333}$	$582^{+477}_{-484}$
2048 Hz	$362^{+378}_{-352}$	$607^{+511}_{-557}$	$320^{+355}_{-305}$	$589^{+399}_{-555}$

On the other hand, for the Hanford data, the unimodal distribution for  $f_{\max} = 1000$  Hz, whose peak is at low- $\tilde{\Lambda}$  region, shrinks for  $f_{\max} = 2048$  Hz. As a result, for  $f_{\max} = 2048$  Hz, the remaining high- $\tilde{\Lambda}$  peak for the Livingston data produces the bump for the HLV combined data. Moreover, a few high- $\tilde{\Lambda}$  bumps in the case of HLV combined data for  $f_{\max} = 2048$  Hz are inherited from the bumps of the Livingston-only data, which are associated with the high-frequency data. The location of the low- $\tilde{\Lambda}$  bump derived by the Livingston-only data is close to the peak of  $\tilde{\Lambda}$  of about 250 derived by the Hanford-only data.

In the case of the TF2+*NRTidalv2* model, as shown in the right panel of Fig. 4, a bump at the high- $\tilde{\Lambda}$  region in the case of HLV combined data for  $f_{\max} = 2048$  Hz are inherited from the peak of the Livingston-only data,  $\tilde{\Lambda} \sim 750$ .

While a bimodal distribution appears in the posterior PDF of  $\tilde{\Lambda}$  with the SEOBNRv4\_ROM\_NRTidal model in the case of LIGO-Virgo analysis as shown in Fig. 11 in [15], a small high- $\tilde{\Lambda}$  bump at  $\tilde{\Lambda} \sim 600$  appears in that with the TF2+*NRTidal* model presented for  $f_{\max} = 2048$  Hz in the right panel of Fig. 3. Here, the SEOBNRv4\_ROM\_NRTidal model is constructed from the SEOBNRv4 model [71, 72] as the BBH baseline and the NRTidal model as the tidal part. Supplementary analysis with the TF2+*NRTidal* model as shown in Fig. 5 demonstrates that the different priors in  $\tilde{\Lambda}$  (one uniform and one non-uniform) make such different distribution between our analysis and the LIGO-Virgo analysis. The LIGO-Virgo collaborations used “Weighted” prior. In this prior, they assume uniform priors in  $\Lambda_1$  and  $\Lambda_2$ , and weight the posterior of  $\tilde{\Lambda}$  by dividing by its prior determined by those of other parameters [15]. “Weighted” prior approximately corresponds to imposing a uniform prior on  $\tilde{\Lambda}$ . Figure 5 shows the dependence of the results on different priors in  $\tilde{\Lambda}$ , “ $\Lambda_{1,2}$ -flat”, “Weighted”, and “ $\tilde{\Lambda}$ -flat” for the TF2+*NRTidal* model with  $f_{\max} = 2048$  Hz. This figure demonstrate that the distribution for “ $\Lambda_{1,2}$ -flat” and “Weighted” prior tends to be a bimodal rather than a high- $\tilde{\Lambda}$  bump.

In Ref. [43], it is found that there is a discrepancy in the estimates of binary tidal deformability of GW170817 be-

tween the Hanford and Livingston detectors of Advanced LIGO by using the restricted TaylorF2 waveform model. Figure 4 shows that the discrepancy is enhanced with sophisticated waveform models (the TF2+*KyotoTidal* and TF2+*NRTidalv2* models). While the two distributions in the cases of the Hanford-only and Livingston-only data seem to be consistent with each other and also consistent with what we would expect from noise realization (e.g., see Ref. [33]), the results that the width of the 90% credible interval for the Livingston-only data does not shrink as  $f_{\max}$  increases indicate that the Livingston’s high-frequency data are not very useful to determine the tidal deformability for GW170817.

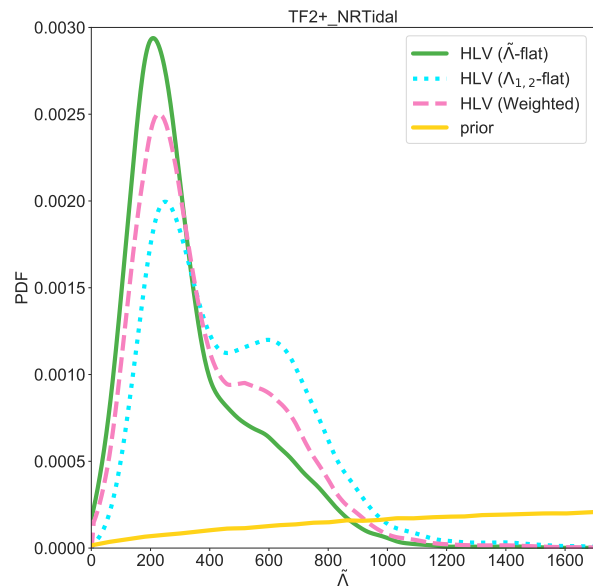


FIG. 5. Dependence of the marginalized posterior PDFs of  $\tilde{\Lambda}$  on different priors in  $\tilde{\Lambda}$  for the TF2+*NRTidal* model with  $f_{\max} = 2048$  Hz. In addition to PDF of  $\tilde{\Lambda}$  for a uniform priors in  $\Lambda_1$  and  $\Lambda_2$  (dotted, cyan), we show the PDF for “Weighted”-prior (dashed, magenta), which is weighted by dividing the original prior (also shown by solid yellow curve) and the PDF for a uniform prior in  $\tilde{\Lambda}$  (solid, green)

- [1] B. P. Abbott *et al.* [LIGO Scientific and Virgo Collaborations], “GW170817: Observation of Gravitational Waves from a Binary Neutron Star Inspiral”, *Phys. Rev. Lett.* **119**, no. 16, 161101 (2017) [arXiv:1710.05832 [gr-qc]].
- [2] B. P. Abbott *et al.*, “Multi-messenger Observations of a Binary Neutron Star Merger,” *Astrophys. J.* **848**, no. 2, L12 (2017) [arXiv:1710.05833 [astro-ph.HE]].
- [3] M. Shibata, S. Fujibayashi, K. Hotokezaka, K. Kiuchi, K. Kyutoku, Y. Sekiguchi and M. Tanaka, “Modeling GW170817 based on numerical relativity and its implications,” *Phys. Rev. D* **96**, no. 12, 123012 (2017) [arXiv:1710.07579 [astro-ph.HE]].
- [4] A. Bauswein, O. Just, H. T. Janka and N. Stergioulas, “Neutron-star radius constraints from GW170817 and future detections,” *Astrophys. J.* **850**, no. 2, L34 (2017) [arXiv:1710.06843 [astro-ph.HE]].
- [5] K. Kiuchi, K. Kyutoku, M. Shibata and K. Taniguchi, “Revisiting the lower bound on tidal deformability derived by AT 2017gfo,” *Astrophys. J.* **876** (2019) no.2, L31 [arXiv:1903.01466 [astro-ph.HE]].
- [6] B. P. Abbott *et al.* [LIGO Scientific and Virgo and Fermi-GBM and INTEGRAL Collaborations], “Gravitational Waves and Gamma-rays from a Binary Neutron Star Merger: GW170817 and GRB 170817A,” *Astrophys. J.* **848**, no. 2, L13 (2017) [arXiv:1710.05834 [astro-ph.HE]].
- [7] B. D. Metzger, T. A. Thompson and E. Quataert, “A magnetar origin for the kilonova ejecta in GW170817,” *Astrophys. J.* **856**, no. 2, 101 (2018) [arXiv:1801.04286 [astro-ph.HE]].
- [8] S. Ai, H. Gao, Z. G. Dai, X. F. Wu, A. Li, B. Zhang and M. Z. Li, “The allowed parameter space of a long-lived neutron star as the merger remnant of GW170817,” *Astrophys. J.* **860**, no. 1, 57 (2018) [arXiv:1802.00571 [astro-ph.HE]].
- [9] S. Z. Li, L. D. Liu, Y. W. Yu and B. Zhang, “What Powered the Optical Transient AT2017gfo Associated with GW170817?,” *Astrophys. J.* **861**, no. 2, L12 (2018) [arXiv:1804.06597 [astro-ph.HE]].
- [10] Y. W. Yu, L. D. Liu and Z. G. Dai, “A long-lived remnant neutron star after GW170817 inferred from its associated kilonova,” *Astrophys. J.* **861**, no. 2, 114 (2018) [arXiv:1711.01898 [astro-ph.HE]].
- [11] B. Margalit and B. D. Metzger, “Constraining the Maximum Mass of Neutron Stars From Multi-Messenger Observations of GW170817,” *Astrophys. J.* **850**, no. 2, L19 (2017) [arXiv:1710.05938 [astro-ph.HE]].
- [12] L. Rezzolla, E. R. Most and L. R. Weih, “Using gravitational-wave observations and quasi-universal relations to constrain the maximum mass of neutron stars,” *Astrophys. J.* **852**, no. 2, L25 (2018) [arXiv:1711.00314 [astro-ph.HE]].
- [13] M. Ruiz, S. L. Shapiro and A. Tsokaros, “GW170817, General Relativistic Magnetohydrodynamic Simulations, and the Neutron Star Maximum Mass,” *Phys. Rev. D* **97**, no. 2, 021501(R) (2018) [arXiv:1711.00473 [astro-ph.HE]].
- [14] M. Shibata, E. Zhou, K. Kiuchi and S. Fujibayashi, “Constraint on the maximum mass of neutron stars using GW170817 event” *Phys. Rev. D* **100**, no. 2, 023015 (2019) [arXiv:1905.03656 [astro-ph.HE]].
- [15] B. P. Abbott *et al.* [LIGO Scientific and Virgo Collaborations], “Properties of the binary neutron star merger GW170817,” *Phys. Rev. X* **9**, no. 1, 011001 (2019) [arXiv:1805.11579 [gr-qc]].
- [16] B. P. Abbott *et al.* [LIGO Scientific and Virgo Collaborations], “GW170817: Measurements of neutron star radii and equation of state”, arXiv:1805.11581 [gr-qc].
- [17] [LIGO Scientific and Virgo Collaborations], “Model comparison from LIGO-Virgo data on GW170817’s binary components and consequences for the merger remnant,” arXiv:1908.01012 [gr-qc].
- [18] W. Kastaun and F. Ohme, “Finite tidal effects in GW170817: observational evidence or model assumptions?,” arXiv:1909.12718 [gr-qc].
- [19] S. De, D. Finstad, J. M. Lattimer, D. A. Brown, E. Berger and C. M. Biwer, “Tidal Deformabilities and Radii of Neutron Stars from the Observation of GW170817,” *Phys. Rev. Lett.* **121**, no. 9, 091102 (2018) Erratum: [*Phys. Rev. Lett.* **121**, no. 25, 259902 (2018)] [arXiv:1804.08583 [astro-ph.HE]].
- [20] C. D. Capano *et al.*, “GW170817: Stringent constraints on neutron-star radii from multimessenger observations and nuclear theory,” arXiv:1908.10352 [astro-ph.HE].
- [21] F. J. Fattoyev, J. Piekarewicz and C. J. Horowitz, “Neutron Skins and Neutron Stars in the Multimessenger Era,” *Phys. Rev. Lett.* **120**, no. 17, 172702 (2018) [arXiv:1711.06615 [nucl-th]].
- [22] E. Annala, T. Gorda, A. Kurkela and A. Vuorinen, “Gravitational-wave constraints on the neutron-star-matter Equation of State,” *Phys. Rev. Lett.* **120**, no. 17, 172703 (2018) [arXiv:1711.02644 [astro-ph.HE]].
- [23] C. Raithel, F. Özel and D. Psaltis, “Tidal deformability from GW170817 as a direct probe of the neutron star radius,” *Astrophys. J.* **857**, no. 2, L23 (2018) [arXiv:1803.07687 [astro-ph.HE]].
- [24] E. P. Zhou, X. Zhou and A. Li, “Constraints on interquark interaction parameters with GW170817 in a binary strange star scenario,” *Phys. Rev. D* **97**, no. 8, 083015 (2018) [arXiv:1711.04312 [astro-ph.HE]].
- [25] V. Paschalidis, K. Yagi, D. Alvarez-Castillo, D. B. Blaschke and A. Sedrakian, “Implications from GW170817 and I-Love-Q relations for relativistic hybrid stars,” *Phys. Rev. D* **97**, no. 8, 084038 (2018) [arXiv:1712.00451 [astro-ph.HE]].
- [26] R. Nandi and P. Char, “Hybrid stars in the light of GW170817,” *Astrophys. J.* **857**, no. 1, 12 (2018) [arXiv:1712.08094 [astro-ph.HE]].
- [27] D. Radice, A. Perego, F. Zappa and S. Bernuzzi, “GW170817: Joint Constraint on the Neutron Star Equation of State from Multimessenger Observations,” *Astrophys. J.* **852**, no. 2, L29 (2018) [arXiv:1711.03647 [astro-ph.HE]].
- [28] E. E. Flanagan and T. Hinderer, “Constraining neutron star tidal Love numbers with gravitational wave detectors,” *Phys. Rev. D* **77**, 021502(R) (2008) [arXiv:0709.1915 [astro-ph]].
- [29] J. Vines, E. E. Flanagan and T. Hinderer, “Post-Newtonian tidal effects in the gravitational waveform from binary inspirals,” *Phys. Rev. D* **83**, 084051 (2011) [arXiv:1101.1673 [gr-qc]].
- [30] M. Favata, “Systematic parameter errors in inspiraling neutron star binaries,” *Phys. Rev. Lett.* **112**, 101101

- (2014) [arXiv:1310.8288 [gr-qc]].
- [31] K. Yagi and N. Yunes, “Love can be Tough to Measure,” *Phys. Rev. D* **89**, no. 2, 021303(R) (2014) [arXiv:1310.8358 [gr-qc]].
- [32] B. D. Lackey and L. Wade, “Reconstructing the neutron star equation of state with gravitational-wave detectors from a realistic population of inspiralling binary neutron stars,” *Phys. Rev. D* **91**, no. 4, 043002 (2015) [arXiv:1410.8866 [gr-qc]].
- [33] L. Wade, J. D. E. Creighton, E. Ochsner, B. D. Lackey, B. F. Farr, T. B. Littenberg and V. Raymond, “Systematic and statistical errors in a bayesian approach to the estimation of the neutron-star equation of state using advanced gravitational wave detectors”, *Phys. Rev. D* **89**, no. 10, 103012 (2014) [arXiv:1402.5156 [gr-qc]].
- [34] T. Damour, A. Nagar and L. Villain, “Measurability of the tidal polarizability of neutron stars in late-inspiral gravitational-wave signals”, *Phys. Rev. D* **85**, 123007 (2012) [arXiv:1203.4352 [gr-qc]].
- [35] T. Hinderer, B. D. Lackey, R. N. Lang and J. S. Read, “Tidal deformability of neutron stars with realistic equations of state and their gravitational wave signatures in binary inspiral,” *Phys. Rev. D* **81**, 123016 (2010) [arXiv:0911.3535 [astro-ph.HE]].
- [36] T. Damour and A. Nagar, “Effective One Body description of tidal effects in inspiralling compact binaries,” *Phys. Rev. D* **81**, 084016 (2010) [arXiv:0911.5041 [gr-qc]].
- [37] D. Bini, T. Damour and G. Faye, “Effective action approach to higher-order relativistic tidal interactions in binary systems and their effective one body description,” *Phys. Rev. D* **85**, 124034 (2012) [arXiv:1202.3565 [gr-qc]].
- [38] D. Bini and T. Damour, “Gravitational self-force corrections to two-body tidal interactions and the effective one-body formalism,” *Phys. Rev. D* **90**, no. 12, 124037 (2014) [arXiv:1409.6933 [gr-qc]].
- [39] S. Bernuzzi, A. Nagar, T. Dietrich and T. Damour, “Modeling the Dynamics of Tidally Interacting Binary Neutron Stars up to the Merger,” *Phys. Rev. Lett.* **114**, no. 16, 161103 (2015) [arXiv:1412.4553 [gr-qc]].
- [40] T. Dietrich, S. Bernuzzi and W. Tichy, “Closed-form tidal approximants for binary neutron star gravitational waveforms constructed from high-resolution numerical relativity simulations”, *Phys. Rev. D* **96**, no. 12, 121501(R) (2017) [arXiv:1706.02969 [gr-qc]].
- [41] T. Dietrich, A. Samajdar, S. Khan, N. K. Johnson-McDaniel, R. Dudi and W. Tichy, “Improving the NR-Tidal model for binary neutron star systems,” *Phys. Rev. D* **100**, no. 4, 044003 (2019) [arXiv:1905.06011 [gr-qc]].
- [42] K. Kawaguchi, K. Kiuchi, K. Kyutoku, Y. Sekiguchi, M. Shibata and K. Taniguchi, “Frequency-domain gravitational waveform models for inspiraling binary neutron stars”, *Phys. Rev. D* **97**, no. 4, 044044 (2018) [arXiv:1802.06518 [gr-qc]].
- [43] T. Narikawa, N. Uchikata, K. Kawaguchi, K. Kiuchi, K. Kyutoku, M. Shibata and H. Tagoshi, “Discrepancy in tidal deformability of GW170817 between the Advanced LIGO twin detectors,” *Phys. Rev. Research* **1**, 033055 (2019) [arXiv:1812.06100 [astro-ph.HE]].
- [44] J. Skilling, *Bayesian Analysis* **1**, 833 (2006).
- [45] J. Veitch and A. Vecchio, “Bayesian coherent analysis of in-spiral gravitational wave signals with a detector network”, *Phys. Rev. D* **81**, 062003 (2010) [arXiv:0911.3820 [astro-ph.CO]].
- [46] J. Veitch, V. Raymond, B. Farr, W. Farr, P. Graff, S. Vitale *et al.*, “Parameter estimation for compact binaries with ground-based gravitational-wave observations using the LALInference software library”, *Phys. Rev. D* **91**, 042003 (2015) [arXiv:1409.7215 [gr-qc]].
- [47] LIGO Scientific Collaboration, “LIGO Algorithm Library LALSuite”, Free Software (GPL), 2018; <https://doi.org/10.7935/GT1W-FZ16>
- [48] A. Buonanno, B. R. Iyer, E. Ochsner, Y. Pan and B. S. Sathyaprakash, “Comparison of post-Newtonian templates for compact binary inspiral signals in gravitational-wave detectors”, *Phys. Rev. D* **80**, 084043 (2009) [arXiv:0907.0700 [gr-qc]].
- [49] L. Blanchet, “Gravitational Radiation from Post-Newtonian Sources and Inspiralling Compact Binaries,” *Living Rev. Rel.* **17**, 2 (2014) [arXiv:1310.1528 [gr-qc]].
- [50] S. Khan, S. Husa, M. Hannam, F. Ohme, M. Pürrer, X. J. Forteza and A. Bohé, “Frequency-domain gravitational waves from nonprecessing black-hole binaries. II. A phenomenological model for the advanced detector era”, *Phys. Rev. D* **93**, no. 4, 044007 (2016) [arXiv:1508.07253 [gr-qc]].
- [51] A. Taracchini *et al.*, “Effective-one-body model for black-hole binaries with generic mass ratios and spins,” *Phys. Rev. D* **89**, no. 6, 061502(R) (2014) [arXiv:1311.2544 [gr-qc]].
- [52] M. Pürrer, “Frequency domain reduced order model of aligned-spin effective-one-body waveforms with generic mass-ratios and spins,” *Phys. Rev. D* **93**, no. 6, 064041 (2016) [arXiv:1512.02248 [gr-qc]].
- [53] A. Bohé, S. Marsat and L. Blanchet, “Next-to-next-to-leading order spin-orbit effects in the gravitational wave flux and orbital phasing of compact binaries”, *Class. Quant. Grav.* **30**, 135009 (2013) [arXiv:1303.7412 [gr-qc]].
- [54] K. G. Arun, A. Buonanno, G. Faye and E. Ochsner, “Higher-order spin effects in the amplitude and phase of gravitational waveforms emitted by inspiraling compact binaries: Ready-to-use gravitational waveforms”, *Phys. Rev. D* **79**, 104023 (2009) Erratum: [*Phys. Rev. D* **84**, 049901 (2011)] [arXiv:0810.5336 [gr-qc]].
- [55] B. Mikoczi, M. Vasuth and L. A. Gergely, “Self-interaction spin effects in inspiralling compact binaries”, *Phys. Rev. D* **71**, 124043 (2005) [astro-ph/0504538].
- [56] T. Hinderer, “Tidal Love numbers of neutron stars,” *Astrophys. J.* **677**, 1216 (2008) [arXiv:0711.2420 [astro-ph]].
- [57] K. Kiuchi, K. Kawaguchi, K. Kyutoku, Y. Sekiguchi, M. Shibata and K. Taniguchi, “Sub-radian-accuracy gravitational waveforms of coalescing binary neutron stars in numerical relativity”, *Phys. Rev. D* **96**, no. 8, 084060 (2017) [arXiv:1708.08926 [astro-ph.HE]].
- [58] T. Hinderer *et al.*, “Effects of neutron-star dynamic tides on gravitational waveforms within the effective-one-body approach,” *Phys. Rev. Lett.* **116**, no. 18, 181101 (2016) [arXiv:1602.00599 [gr-qc]].
- [59] J. Steinhoff, T. Hinderer, A. Buonanno and A. Taracchini, “Dynamical Tides in General Relativity: Effective Action and Effective-One-Body Hamiltonian,” *Phys. Rev. D* **94**, no. 10, 104028 (2016) [arXiv:1608.01907 [gr-qc]].
- [60] B. D. Lackey, M. Pürrer, A. Taracchini and S. Marsat, “Surrogate model for an aligned-spin effective one body waveform model of binary neutron star inspirals using Gaussian process regression,” *Phys. Rev. D* **100**, no. 2,

- 024002 (2019) [arXiv:1812.08643 [gr-qc]].
- [61] M. Soares-Santos *et al.* [DES and Dark Energy Camera GW-EM Collaborations], “The Electromagnetic Counterpart of the Binary Neutron Star Merger LIGO/Virgo GW170817. I. Discovery of the Optical Counterpart Using the Dark Energy Camera,” *Astrophys. J.* **848**, no. 2, L16 (2017) [arXiv:1710.05459 [astro-ph.HE]].
- [62] M. Burgay *et al.*, “An Increased estimate of the merger rate of double neutron stars from observations of a highly relativistic system,” *Nature* **426**, 531 (2003) [astro-ph/0312071].
- [63] K. Stovall *et al.*, “PALFA Discovery of a Highly Relativistic Double Neutron Star Binary,” *Astrophys. J.* **854**, no. 2, L22 (2018) [arXiv:1802.01707 [astro-ph.HE]].
- [64] B. P. Abbott *et al.* [LIGO Scientific and Virgo Collaborations], “GWTC-1: A Gravitational-Wave Transient Catalog of Compact Binary Mergers Observed by LIGO and Virgo during the First and Second Observing Runs,” arXiv:1811.12907 [astro-ph.HE].
- [65] A. Samajdar and T. Dietrich, “Waveform systematics for binary neutron star gravitational wave signals: effects of the point-particle baseline and tidal descriptions,” *Phys. Rev. D* **98**, no. 12, 124030 (2018) [arXiv:1810.03936 [gr-qc]].
- [66] A. Samajdar and T. Dietrich, “Waveform systematics for binary neutron star gravitational wave signals: Effects of spin, precession, and the observation of electromagnetic counterparts,” arXiv:1905.03118 [gr-qc].
- [67] S. Hild, S. Chelkowski and A. Freise, “Pushing towards the ET sensitivity using ‘conventional’ technology,” arXiv:0810.0604 [gr-qc].
- [68] M. Punturo *et al.*, “The Einstein Telescope: A third-generation gravitational wave observatory,” *Class. Quant. Grav.* **27**, 194002 (2010).
- [69] S. Ballmer and V. Mandic, “New Technologies in Gravitational-Wave Detection,” *Ann. Rev. Nucl. Part. Sci.* **65**, 555 (2015).
- [70] B. P. Abbott *et al.* [LIGO Scientific Collaboration], “Exploring the Sensitivity of Next Generation Gravitational Wave Detectors,” *Class. Quant. Grav.* **34**, no. 4, 044001 (2017) [arXiv:1607.08697 [astro-ph.IM]].
- [71] A. Bohé, L. Shao, A. Taracchini, A. Buonanno, S. Babak, I. W. Harry *et al.*, “Improved effective-one-body model of spinning, nonprecessing binary black holes for the era of gravitational-wave astrophysics with advanced detectors,” *Phys. Rev. D* **95**, no. 4, 044028 (2017) [arXiv:1611.03703 [gr-qc]].
- [72] M. Pürrer, “Frequency domain reduced order models for gravitational waves from aligned-spin compact binaries,” *Class. Quant. Grav.* **31**, no. 19, 195010 (2014) [arXiv:1402.4146 [gr-qc]].